# Interactions and dynamics of the Shine–Dalgarno helix in the 70S ribosome

**Andrei Korostelev, Sergei Trakhanov, Haruichi Asahara, Martin Laurberg, Laura Lancaster, and Harry F. Noller†**

Center for Molecular Biology of RNA and Department of Molecular, Cell and Developmental Biology, University of California, Santa Cruz, CA 95060

Contributed by Harry F. Noller, August 29, 2007 (sent for review April 30, 2007)

**The crystal structure of an initiation-like 70S ribosome complex containing an 8-bp Shine–Dalgarno (SD) helix was determined at 3.8-Å resolution. Translation–libration–screw analysis showed that the inherent anisotropic motions of the SD helix were biased along its helical axis, suggesting that during the first step of translocation, the SD helix moves along its helical screw axis. Contacts between the SD helix and the ribosome were primarily through interactions with helices 23a, 26, and 28 of 16S rRNA. Contact with the neck (helix 28) of the 30S subunit near its hinge point suggests that formation of the SD helix could affect positioning of the head of the 30S subunit for optimal interaction with initiator tRNA. The bulged U723 in helix 23a interacts with the minor groove of the SD helix at the C1539·G-10 base pair, explaining its selective conservation in bacteria and archaea.**

mRNA | ribosome structure | rRNA | translation–libration–screw analysis | x-ray crystallography

During initiation of protein synthesis, mRNA and tRNA are optimally positioned on the 30S subunit, with the help of initiation factors, before association with the 50S subunit to form the complete 70S initiation complex (1). For most mRNAs, selection of the correct start codon and translational reading frame depend on base pairing between a sequence upstream from the initiator codon in the mRNA [the Shine–Dalgarno (SD) sequence] and a conserved CCUCC sequence in the 3′ tail of 16S rRNA (the anti-SD sequence) (1, 2). However, relatively little is known about how formation of the SD helix affects the conformation of the ribosome and its functional interactions during initiation. The path of mRNA through the ribosome and location of the SD helix were first visualized by x-ray crystallography at 7-Å resolution (3). In recent 4.5- to 5.5-Å crystal structures of the *Thermus thermophilus* 70S ribosome (4), the orientation of the SD helix in an initiation-like complex, formed with a mRNA in which the central A of the SD sequence is at position −8 relative to the initial A of the start codon, was rotated by 70° from that in a 70S elongation-like complex containing mRNA with an SD sequence centered on position −13.

## Results and Discussion

We determined the structure of an initiation-like 70S ribosomal complex at 3.8-Å resolution, in which the SD helix is well resolved (Fig. 1). The complex contained an initiator $tRNA^{fMet}$ bound to the P site, endogenous elongator tRNAs bound to the E site, and a defined 27-nucleotide mRNA (3) containing an 8-nt SD sequence centered at position −8. The final steps of structure determination involved translation–libration–screw (TLS) refinement (5), which offers an opportunity to interpret anisotropic movements of rigid domains by using the experimental x-ray diffraction data (6, 7). Refined TLS parameters were validated against those obtained for the previously published 3.7-Å crystal structure of a different 70S ribosome complex (8). Remarkably, the position of the dominant screw axis showed that the inherent anisotropic motions of the SD helix were strongly biased along its helical axis (Fig. 1 *b* and *c*). This suggests that in the first step of translocation following initiation, the SD helix undergoes a screw-like movement along its axis, consistent with the orientation of the SD helix in an elongation-like complex (Fig. 2). The orientation of the SD helix in our initiation-like complex was similar to that observed in a recently determined structure of the 30S subunit in which an RNA oligonucleotide is bound to the 3′ end of 16S rRNA to mimic the SD helix (9). This position contrasts with that reported for a very similar 70S complex (4), in which the SD helix was rotated by 70°, in an orientation similar to that observed previously at 7-Å resolution (3). The basis of this difference is not clear, because the mRNAs used in the two kinds of complexes are nearly identical, differing in only two nucleotides at positions +5 and +6 and were formed by using ribosomes and tRNAs from the same sources. Differences between crystal forms and crystallization conditions are potential contributing factors. Electron density for the 4-nt linker between the SD-forming bases and the initiator codon positioned at the P site is not well defined; however, phosphate groups could be identified. The average distance between phosphate groups in the linker is 6.5 Å, which is nearly the same as that in the similar 70S ribosomal complex (4); this may indicate that no additional strain is created when the SD helix and the initiator codon are positioned as reported in this study. However, a higher-resolution structure and/or molecular dynamics simulations are necessary to address this issue. In any case, it is clear that models for the postinitiation phase of translation need to take into account the observation that the SD helix in an initiation-like complex can occupy the same position as that in an elongation-like complex (Fig. 2*b*).

Accurate positioning of the SD helix allows for detailed visualization of its interactions with specific structural features of the ribosome, with implications for additional influences on the initiation process (Fig. 3*a*). The backbone of the SD helix around A1534 packs against the neck of the 30S subunit (helix 28 of 16S rRNA) near G929, which has been identified as a hinge point for movement of the head of the 30S subunit (10). On its opposite face, positions 1539–1541 of the SD helix interact with the platform of the small subunit, packing against helix 23a and along the minor groove of helix 26 of 16S rRNA (Fig. 3*b*). The bulged nucleotide U723 of helix 23a is positioned to interact with the minor-groove side of the C1539·G-10 base pair of the SD helix (Fig. 3*b*); however, electron density for the U723 base is not strong enough to provide the details of this interaction. Interaction of U723 with the SD helix explains why it is selectively conserved in bacteria and archaea (11), the 16S rRNAs of which contain anti-SD sequences. To accommodate the SD helix, h26 and h28 move apart by more than 2 Å relative to their positions in the vacant 70S ribosome (10). This modest displacement near the hinge point of the neck results in a 13-Å change in the

Author contributions: A.K. and S.T. contributed equally to this work; A.K. and S.T. designed research; A.K., S.T., H.A., and M.L. performed research; S.T., H.A., M.L., and L.L. contributed new reagents/analytic tools; A.K. and H.F.N. analyzed data; and A.K. and H.F.N. wrote the paper.

The authors declare no conflict of interest.

Abbreviations: SD, Shine–Dalgarno; TLS, translation–libration–screw.

Data deposition: The atomic coordinates and structure factors have been deposited in the Protein Data Bank, www.pdb.org (PDB ID code 2QNH).

†To whom correspondence should be addressed. E-mail: harry@nuvolari.ucsc.edu.

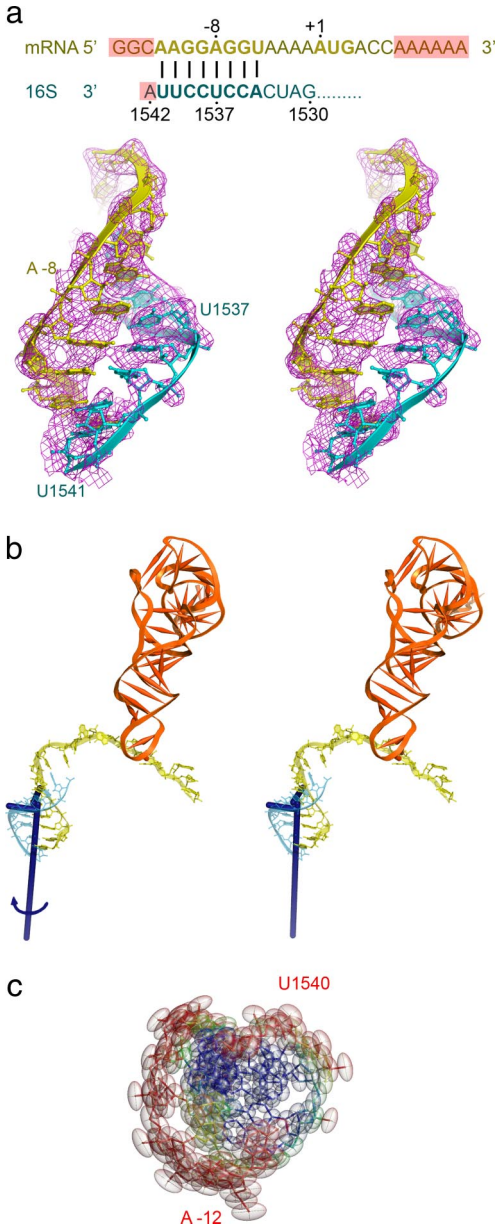


**Fig. 1.** Structure and dynamics of the SD helix. (*a*) (*Upper*) Nucleotide sequences and base pairing between mRNA and 16S rRNA in the initiation-like 70S ribosome complex. SD sequence, initiator codon, and anti-SD sequences are shown in bold; shaded nucleotides are disordered in the refined x-ray structure. (*Lower*) Stereoview of the fit of the SD helix to a composite omit density map calculated with $\sigma_A$-weighted ($2F_o - F_c$) coefficients contoured at 1.2$\sigma$. (*b*) Stereoview of the nonintersecting screw axes (blue) for the SD helix (yellow). The length of each axis is proportional to its respective mean-square displacement value. The primary screw axis is indicated by a rotational arrow. (*c*) Thermal ellipsoid representation of the librational motions of the SD helix around the dominant screw axis coinciding with the SD helical axis. Atomic displacement parameters for the SD helix calculated from the TLS model are colored according to the magnitude of the displacements, increasing from blue (smallest) to red (largest). The view is from the upstream end of the helix.

positions of nucleotides G1338 and A1339 in the head of the subunit, which make critical A-minor-type interactions with the anticodon stem of initiator $tRNA^{fMet}$ (10, 12). Comparison of TLS parameters for the current structure with those of our previous 3.7-Å structure of a similar complex lacking a SD helix (8) suggests that the presence of the SD helix reduces the mobility of the head and platform, whereas the rest of the 16S

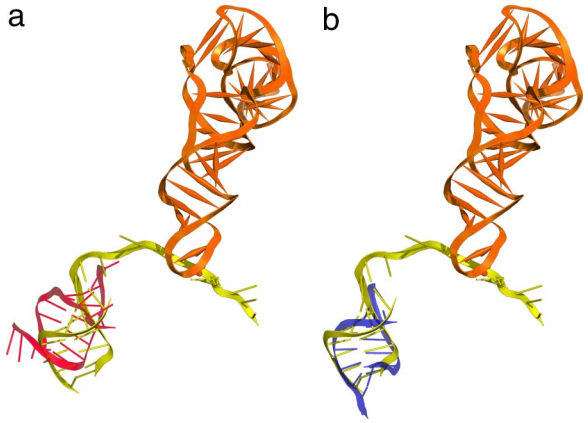


**Fig. 2.** Comparison of the positions of the SD helices. (*a* and *b*) Positions of the SD helices in the 3.8-Å (yellow) and 4.5-Å (4) (red) initiation-like complex (*a*) and 5.5 Å elongation-like complex (4) (blue) (*b*) relative to the P-site tRNA (orange).

and the 23S rRNAs demonstrate similar mobility between the structures. Thus, positioning of the SD helix may help to fix the orientation of the mobile head of the 30S subunit (10, 13) for optimal interaction with $tRNA^{fMet}$ at the 30S P site during initiation.

Among the small subunit proteins, the basic N-terminal tail of S18 makes extensive contacts with the backbone of the 16S rRNA strand of the SD helix around nucleotides 1536–1539. Based on the structure of the vacant *Escherichia coli* 70S ribosome, the SD helix would clash sterically with protein S21, which has no analog in *T. Thermophilus*. Thus, if the SD helix were to adopt a similar orientation in the *E. coli* 70S initiation complex, S21 would need to move. Because S21 has been reported to play a role in initiation on SD-containing mRNAs in *E. coli* (14), its function may be to modulate interactions between the SD helix and 16S rRNA.

## Materials and Methods

**Ribosome Preparation and Crystallization.** *T. thermophilus* 70S ribosomes were isolated as described previously (15, 16), recrystallized three times with 10–15% 2-methyl-2,4-pentanediol (MPD), and dissolved in a mixture containing 25 mM K–Hepes (pH 7.5), 12.5 mM Na–cacodylate (pH 5.5), 2.5 mM Tris·HCl (pH 7.5), 80 mM $NH_4Cl$, 80 mM KCl, 11 mM $MgCl_2$, 6.5 mM thermine·HCl, and 0.2 M KSCN. Complexes were formed in a volume of 30 $\mu$l with 70S ribosomes (13 mg/ml)/EF–Tu ternary complex/MT27 mRNA/fMet–$tRNA^{fMet}$ in a ratio of 1:1.9:1:1. Electron density for the EF–Tu ternary complex was absent following structure refinement. The mixture was incubated for 24 h at 30°C before crystallization by the hanging drop method over 26–30% MPD in the abovementioned buffer mix by using 2 $\mu$l of ribosome complex mixed with 2 $\mu$l of well mixture on siliconized cover slips. Crystallization was nucleated for 1 week at room temperature and then incubated at 16°C for 3 weeks before transferring to the cold room for mounting. Crystals were flash cooled according to the procedure described by Sargent and Richmond (17). All crystal handling was performed in the cold room to minimize dehydration of the crystals. An individual ribosome crystal obtained from a 0.2-mm loop assemblage with magnetic base (Hampton Research) was immediately placed in a 1.5-ml Eppendorf tube over 55% MPD in the abovementioned buffer mix. (The inner diameter of the collar of the Eppendorf tube coincides with the diameter of the magnetic base, providing tight contact and preventing evaporation.) Ten Eppendorf tubes containing crystals were placed in an aluminum heating block preequilibrated to cold room temperature and transferred to −20°C to obtain gradual cooling over 1 h. Crystals were then plunged into

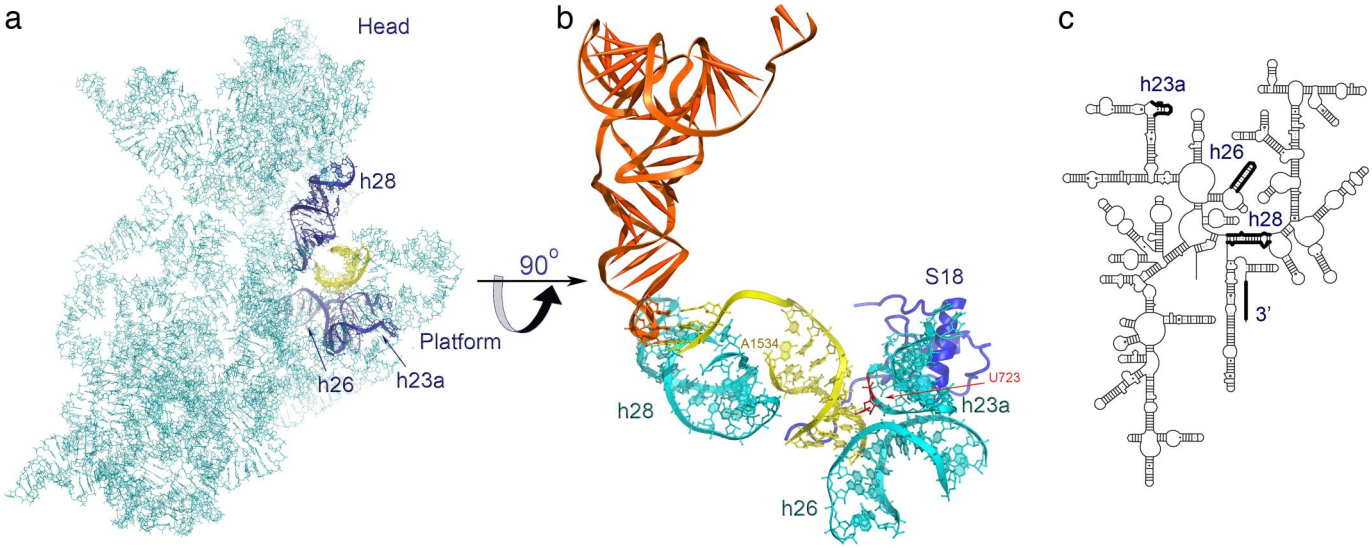


**Fig. 3.** Interactions of the SD helix with the ribosome. (*a*) Location of the SD helix (yellow) relative to the structure of 16S rRNA in the 70S ribosome initiation-like complex. Helices 23a, 26, and 28, which contact the SD helix, are rendered in dark blue ribbon representations, and the SD helix is shown in yellow. (*b*) Interactions of the SD helix with helices 23a, 26, and 28 of 16S rRNA. The P-site tRNA is shown in orange. (*c*) Secondary structure of *T. thermophilus* 16S rRNA, showing in bold the anti-SD region at the 3′ end and structural features (helices 23a, 26, and 28) that interact with the SD helix.

crystal caps containing liquid propane at −120°C and then immersed in liquid nitrogen and stored in a Dewar flask for data collection.

**Structure Determination.** X-ray diffraction data were collected at Beamline 12.3.1 at the Advanced Light Source at Lawrence Berkeley National Laboratory (Berkeley, CA) by using an x-ray wavelength of 0.9835 Å and an oscillation angle of 0.3°. They were integrated with D*TREK (18) and scaled with SCALA (19). Although data completeness is significantly lower for the outer resolution shell than the overall completeness (Table 1), it is not uncommon to use diffraction data with completeness of 75% or less for the entire dataset (20–24) and of 20–45% for the highest-resolution shell (22–25), especially when experimental data or a higher-resolution structure is available for phasing. It has been shown that inclusion of weaker high-resolution reflections improves maximum-likelihood-based refinements (26) because it significantly increases the amount of unique data against which the model is refined. The behavior of $\sigma_A$ as a function of resolution, calculated from test-set reflections (26, 27), which were not used during refinement, independently showed that the effective resolution cutoff was 3.8 Å (Fig. 4). Composite omit maps were used for model building and real-space refinements (28) to minimize model bias (29). A 3.7-Å structure of the ribosome (8) with ribosomal proteins L15, L19, L21, L28, and L29 adapted from the recent 2.8-Å 70S ribosome structure (30) was used as a starting model. The SD helix was not modeled until the final stage of refinement to exclude model bias. The structure was refined as described by Korostelev *et al.* (8), yielding $R/R_{free}$ of 0.327/0.351 and good stereochemistry (Table 1). REFMAC (5) and TLSANL (31) were used for TLS refinement and interpretation of the results. Refined TLS parameters of ribosomal components not including the SD helix were consistent with those found for the 3.7-Å ribosome structure (8), indicating that they can be interpreted in terms of anisotropic domain motion (32). PyMoL (DeLano Scientific LLC, Palo Alto, CA) and Rastep3D (33) were used for figure preparation.

**Table 1. Summary of crystallographic data and refinement**

| | |
|---|---|
| Data statistics | |
| Space group | *I*422 |
| Unit cell dimensions, Å | $a = b = 507.2$, $c = 692.5$ |
| Resolution, Å | 3.83–78 Å (4.04) |
| No. of unique reflections | 354,761 (14,587) |
| Completeness, % | 82.0 (37.7) |
| Multiplicity | 5.0 (1.8) |
| Mean $I/\sigma(I)$ | 3.4 (1.4) |
| $R_{pim}$ | 0.150 (0.452) |
| Refinement statistics | |
| Resolution, Å | 3.83–30.0 |
| Test-set (free) reflections, % | 2.5 |
| $R/R_{free}$ | 0.327/0.351 |
| Deviation from ideal bond lengths, Å | 0.009 |
| Deviation from ideal bond angles, ° | 1.237 |

Statistics for the highest-resolution shell are given in parentheses. $R_{pim}$ denotes the precision-indicating merging *R* factor (34). All measured reflections were used in refinements with CNS (35) and REFMAC (5).

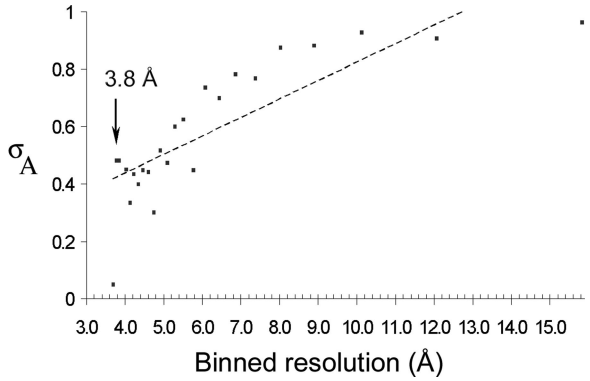


**Fig. 4.** Plot of cross-validated $\sigma_A$ vs. resolution for the 70S ribosome complex. The subset of the diffraction data used for the calculation of the free *R* value was used for computation of $\sigma_A$. The continuous line was obtained by linear fit, and the arrow at 3.8 Å indicates the resolution at which $\sigma_A$ drops sharply from its previous value. This resolution was taken as the effective resolution limit of the diffraction data useful for structure refinement.

We thank Albion Baucom for assistance with data collection and William Scott for help with data processing. We thank the staff of Beamline 5.0.2 at the Advanced Light Source, Lawrence Berkeley National Laboratory (Berkeley, CA), for support during data collection. This work was supported by National Institutes of Health Grants GM-17129 and GM-59140 (to H.F.N.).

1. Gold L, Pribnow D, Schneider T, Shinedling S, Singer BS, Stormo G (1981) *Annu Rev Microbiol* 35:365–403.
2. Shine J, Dalgarno L (1974) *Proc Natl Acad Sci USA* 71:1342–1346.
3. Yusupova GZ, Yusupov M, Cate JHD, Noller HF (2001) *Cell* 106:233–241.
4. Yusupova G, Jenner L, Rees B, Moras D, Yusupov M (2006) *Nature* 444:391–394.
5. Winn MD, Murshudov GN, Papiz MZ (2003) *Methods Enzymol* 374:300–321.
6. Yousef MS, Fabiola F, Gattis JL, Somasundaram T, Chapman MS (2002) *Acta Crystallogr D Biol Crystallogr* 58:2009–2017.
7. Chaudhry C, Horwich AL, Brunger AT, Adams PD (2004) *J Mol Biol* 342:229–245.
8. Korostelev A, Trakhanov S, Laurberg M, Noller HF (2006) *Cell* 126:1065–1077.
9. Kaminishi T, Wilson DN, Takemoto C, Harms JM, Kawazoe M, Schluenzen F, Hanawa-Suetsugu K, Shirouzu M, Fucini P, Yokoyama S (2007) *Structure (London)* 15:289–297.
10. Schuwirth BS, Borovinskaya MA, Hau CW, Zhang W, Vila-Sanjurjo A, Holton JM, Cate JH (2005) *Science* 310:827–834.
11. Cannone JJ, Subramanian S, Schnare MN, Collett JR, D'Souza LM, Du Y, Feng B, Lin N, Madabusi LV, Muller KM, *et al.* (2002) *BMC Bioinformatics* 3:2.
12. Lancaster L, Noller HF (2005) *Mol Cell* 20:623–632.
13. Gao H, Sengupta J, Valle M, Korostelev A, Eswar N, Stagg SM, Van Roey P, Agrawal RK, Harvey SC, Sali A, *et al.* (2003) *Cell* 113:789–801.
14. Van Duin J, Wijnands R (1981) *Eur J Biochem* 118:615–619.
15. Gogia ZV, Yusupov MM, Spirina TN (1986) *Mol Biol (Moscow)* 20:519–525.
16. Collaborative Computational Project, Number 4 (1994) *Acta Crystallogr D Biol Crystallogr* 50:760–763.
17. Sargent DF, Richmond TJ (2004) *Acta Crystallogr D Biol Crystallogr* 60:616 (lett).
18. Pflugrath JW (1999) *Acta Crystallogr D Biol Crystallogr* 55:1718–1725.
19. Evans P (2006) *Acta Crystallogr D Biol Crystallogr* 62:72–82.
20. Berk V, Zhang W, Pai RD, Cate JH (2006) *Proc Natl Acad Sci USA* 103:15830–15834.
21. Su S, Gao YG, Robinson H, Liaw YC, Edmondson SP, Shriver JW, Wang AH (2000) *J Mol Biol* 303:395–403.
22. Xu H, Yang C, Chen L, Kataeva IA, Tempel W, Lee D, Habel JE, Nguyen D, Pflugrath JW, Ferrara JD, *et al.* (2005) *Acta Crystallogr D Biol Crystallogr* 61:960–966.
23. Komori H, Satomoto K, Ueda Y, Shibata N, Inagaki S, Yoshioka S, Aono S, Higuchi Y (2006) *Acta Crystallogr Sect F Struct Biol Cryst Commun* 62:471–473.
24. Alexopoulos E, Kusel A, Sheldrick GM, Diederichsen U, Uson I (2004) *Acta Crystallogr D Biol Crystallogr* 60:1971–1980.
25. Johansson K, El-Ahmad M, Ramaswamy S, Hjelmqvist L, Jornvall H, Eklund H (1998) *Protein Sci* 7:2106–2117.
26. DeLaBarre B, Brunger AT (2006) *Acta Crystallogr D Biol Crystallogr* 62:923–932.
27. Ling H, Boodhoo A, Hazes B, Cummings MD, Armstrong GD, Brunton JL, Read RJ (1998) *Biochemistry* 37:1777–1788.
28. Korostelev A, Bertram R, Chapman MS (2002) *Acta Crystallogr D Biol Crystallogr* 58:761–767.
29. Hodel A, Kim SH, Brünger AT (1992) *Acta Crystallogr A* 48:851–858.
30. Selmer M, Dunham CM, Murphy FVT, Weixlbaumer A, Petry S, Kelley AC, Weir JR, Ramakrishnan V (2006) *Science* 313:1935–1942.
31. Howlin B, Butler SA, Moss DS, Harris GW, Driessen HPC (1993) *J Appl Crystallogr* 26:622–624.
32. Korostelev A, Noller MF (August 29, 2007) *J Mol Biol*, 10.1016/j.jmb.2007.08.054.
33. Merritt B (1997) *Methods Enzymol* 277:505–524.
34. Weiss MS (2001) *J Appl Crystallogr* 130–135.
35. Brünger AT, Adams PD, Clore GM, DeLano WL, Gros P, Grosse-Kunstleve RW, Jiang JS, Kuszewski J, Nilges M, Pannu NS, *et al.* (1998) *Acta Crystallogr D Biol Crystallogr* 54:905–921.